

Flexible Transistors with High Carrier Mobilities Made from Carbon Nanotubes

Organic-based electronics are of great interest as a replacement for inorganic semiconductor devices, as the former are inexpensive, lightweight, and flexible, allowing the development of large flexible displays and electronic paper. However, progress in integrated organic-based electronic devices has been slow due to the low charge-carrier mobilities of these materials, which typically range from $\sim 0.1 \text{ cm}^2/\text{V s}$ —for example, poly(3-hexylthiophene)—to a maximum of $\sim 2 \text{ cm}^2/\text{V s}$ for the best *p*-type crystalline organic semiconductors, with *n*-type carrier mobilities even lower. Carbon nanotubes show promise in overcoming these limitations because their carrier mobility exceeds even common semiconductor materials. Not only do carbon nanotubes exhibit very high strength, but their flexibility makes them a promising material for the development of large-scale flexible electronics. A team of researchers from Nanomix Inc. in Emeryville, Calif., recently demonstrated carbon nanotube-based *p*-type transistor networks supported on a flexible polymer substrate with an order of magnitude increase in hole-carrier mobility.

As reported in the October issue of *Nano Letters*, K. Bradley, J.-C.P. Gabriel, and G. Grüner of Nanomix manufactured and tested carbon nanotube network transistors on flexible polymer substrates. These polymer-supported networks show high durability during repeated bending and exhibit a hole-carrier mobility of $12 \text{ cm}^2/\text{V s}$. The researchers used chemical vapor deposition to grow the carbon nanotube networks on 200-nm-thick silicon oxide layers on a Si substrate that consist of randomly oriented individual nanotubes rather than bundles. Using conventional lithography, the researchers patterned Ti/Au source/drain contacts onto the nanotube networks (3.5 nm Ti followed by 50 nm Au; 200 μm pads separated by 50 μm gaps), resulting in a field-effect transistor network with on/off ratios as high as 10^4 . The scientists transferred the semiconducting networks to a flexible polymer substrate by spin-coating a 15 μm polyimide film as the polymer support onto the silicon substrate, followed by a HF etch step to remove the SiO_2 layer to induce device lift-off.

The devices were tested for their performance by placing the polyimide films on a metal chuck, which served as the gate electrode. The resulting device transfer characteristics exhibited large modulations in conductance for voltages of less than 100 V, confirming that the polymer-

supported networks behave as field-effect transistors. For a dielectric film as thick as 15 μm , these switching voltages are remarkably low, according to the researchers. The research team said that the low switching voltage is due to the high carrier mobility of the carbon nanotube network, with a measured hole mobility of $12 \text{ cm}^2/\text{V s}$. This mobility is an order of magnitude improvement over the best currently used organic materials. The flexible network devices are remarkably resilient: A 60° bending produces only a 12% decrease in conductance with full recovery over 12 bending cycles performed, despite the presence of multiple nanotube–nanotube junctions. The fabricated polymer-supported network transistors exhibit electronic properties that are similar to those of more conventional, silicon-supported carbon nanotube devices; they are flexible and could be made inexpensively.

ALFRED A. ZINN

Fluorescence from Individual Single-Walled Carbon Nanotubes Is Not Intermittent

Potential photonic applications of single-walled carbon nanotubes (SWNTs) in-

clude nanometer-scaled integrated electroluminescent devices. Development of nanodevices, by their very nature, would benefit from the determination of specific optical properties of individual molecules, such as the true spectral linewidth. Until now, only ensemble-averaged spectra of SWNTs, in which spectral details are obscured, have been reported. However, a research team has reported fluorescence spectra from individual SWNTs. Their findings were published in the September 5 issue of *Science*.

University of Rochester and Universität Siegen researcher A. Hartschuh, together with a team of researchers, isolated individual nanotubes by spin-coating a SWNT suspension onto a glass coverslip. Atomic force microscopy showed that short SWNTs, with lengths of 200–300 nm, predominated. A density of about 10–20 Raman-active nanotubes per $100 \mu\text{m}^2$ was determined with confocal Raman imaging. Laser excitation at 633 nm ensured that Raman signals (between 633 nm and 770 nm) were isolated from the fluorescence signals above 850 nm.

Using simultaneous resonance Raman and fluorescence measurements, the researchers found that individual nanotubes

GLASSMAN HIGH VOLTAGE DC Power Supply Solutions for Vacuum Processing Applications

For small DC Sputtering sources, DC bias, Ion sources and Glow Discharge Plasma Requirements

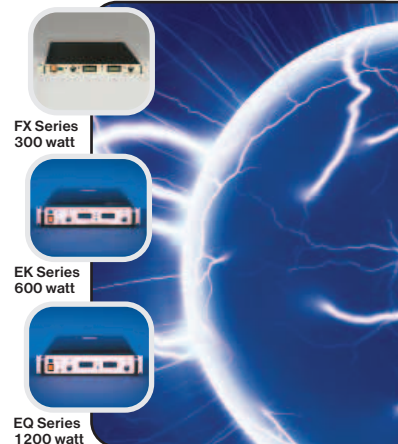
For over 25 years the Glassman name is synonymous with High Reliability Performance and has built its reputation as a market leader by its dedication and investment in technology development as well as after-sale customer support that is second to none in the power supply industry.

For Vacuum processing applications, Glassman's FX(300W), EK(600W) and EQ(1.2kW) series power supplies will meet your needs for low-mid power requirements, with typical application output voltage range from 300V-10kV. All feature compact size, advanced arc management, low stored energy, and use air as the primary dielectric—**A Glassman Innovation!**

Key Features:

- Proprietary Arc Sense and Arc Quench circuitry for ultimate power supply and load protection
- High frequency technology—up to 60kHz
- Tight regulation and high stability
- Low stored output energy
- RS-232 serial interface option

For more information on the complete line of Glassman High Voltage power supplies, visit our website at www.glassmanhv.com or call us today at 908-638-3800.



Check out our new website
www.glassmanhv.com

GLASSMAN HIGH VOLTAGE INC.
Designing Solutions for High Voltage and Vacuum Processing DC Power Supply Applications

Glassman High Voltage, Inc., 124 West Main Street,
PO Box 317, High Bridge, NJ 08829-0317
Phone: (908) 638-3800, FAX: (908) 638-3700

www.glassmanhv.com email: sales@glassmanhv.com

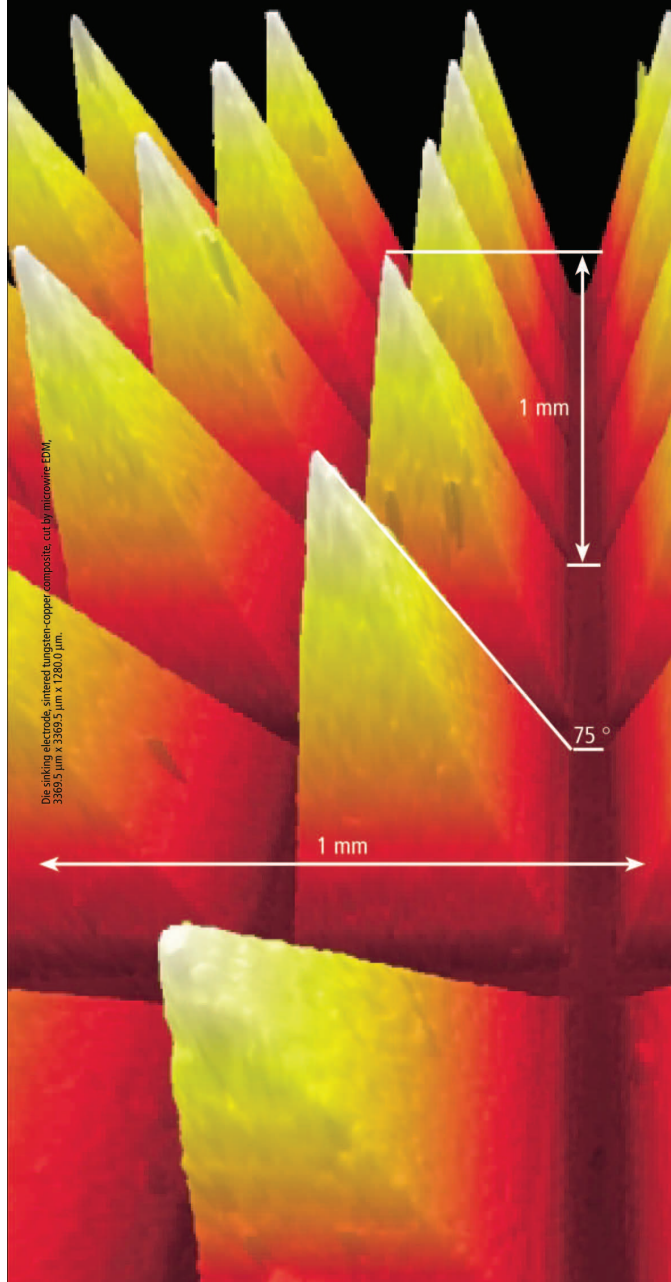
In Europe, Glassman Europe Limited
(UK) +44 1256 883007, FAX: +44 1256 883017
In Asia, Glassman Japan Limited +81 45 902 9988,
FAX: +81 45 902 2268

For more information, see <http://advertisers.mrs.org>

Know the Ups and Downs ...

Steep slope
+ Big height difference
+ Large scan field

The LSM 5 PASCAL confocal laser scanning microscope broadens your microscopic horizons.



Die sinking electrode, sintered tungsten-copper composite, cut by microwave EDM, 3869.5 μm x 3869.5 μm x 1280.0 μm .

Highly resolved images.
Simple and efficient imaging.
Non-destructive.

www.zeiss.com/lsm-mat



We make it visible.

with identical structures—that is, identical diameters and chiralities—display different emission energies, although each individual emission line does match transitions observed in ensemble-averaged spectra. The researchers used low-energy Raman scattering attributed to the nanotube's radial breathing mode to verify that the source of the fluorescence was individual nanotubes. The researchers attribute the heterogeneous emission properties obtained from SWNTs with identical diameter and chirality values to localized defects and perturbations.

For moderate excitation energies ($<70 \text{ kW cm}^{-2}$), time traces of the fluorescence of individual SWNTs showed constant amplitude for 100 s. The researchers said that by contrast both molecular dyes and individual semiconducting quantum dots exhibit fluorescence emission intermittencies or an on/off blinking behavior over very long time scales. The researchers conclude that "SWNTs have the potential to provide a stable, single-molecule infrared photon source with extremely narrow linewidth."

STEVEN TROHALAKI

Three-Phase Boundary Fuel-Cell Reactor Produces H_2O_2 at 93% Selectivity

Industrial production of hydrogen peroxide (H_2O_2) requires separation and distillation from a solution of alkylated anthraquinones (from crude oil) in a multistep procedure that consumes a lot of energy. For certain applications, a costly electrolysis process is used, but this option is not commonplace for high-scale production. Uses of H_2O_2 include water and wastewater treatment, bleaching of textiles and paper, food processing, and even odor control. To create a cost-effective and energy-efficient system suitable for large-scale production of H_2O_2 , I. Yamanaka and his colleagues at the Tokyo Institute of Technology have designed a fuel-cell reactor with a three-phase boundary that overcomes the disadvantages of previous designs. With a three-phase boundary formed by gaseous O_2 , aqueous electrolyte, and a solid porous cathode, this reactor reduces the chance of O_2 and H_2 coming into contact and exploding; it generates electricity along with H_2O_2 .

As reported in the August 8 issue of *Angewandte Chemie*, both the cathode and anode were fabricated from hot-pressed vapor-grown carbon fiber and poly(tetrafluoroethylene) powder, adding a small amount of a carbon black material to the cathode and platinum black powder to the anode. Pure O_2 and H_2 are the starting gases, and titration against KMnO_4 determined the concentration of H_2O_2 . A cation membrane separated the electrolyte compartment between the cathode and the anode into two sections, each one filled with NaOH . Diffusion of H_2O to the cathode compartment under stagnant conditions depleted the anode compartment and reduced the current density. Pumping NaOH continuously into the anode compartment helped stabilize the current density. Electrochemical measurements determined that the rate-controlling reaction was the reduction of O_2 . Using this reactor, H_2O_2 selectivity based on H_2 or current efficiency based on the two-electron reaction is 93% after 2 h, the rate of formation is 2.0 mmol/h cm^2 , the concentration is 7.0 wt%, and the current density is 100 mA/cm^2 , similar to that obtained by electrolysis ($80\text{--}120 \text{ mA/cm}^2$). By substituting O_2 for air, the current efficiency is 88% after 3 h, the rate of formation is 1.3 mmol/h cm^2 , the concentration is 6.5 wt%, and the current density is 78 mA/cm^2 , which is a slight decrease but still a good performance yet less expensive, representing an advantage for industrial-scale production.

SIARI SOSA

Single-Molecule Resistance Measured by Repeated Formation of Molecular Junctions

In the process of using individual molecules to create electronic circuits, the resistance level of a simple molecule like an alkane

chain covalently attached to two electrodes is still a subject of debate. B. Xu and N.J. Tao from Arizona State University have measured the resistance of single molecules by repeatedly forming molecular junctions

between a gold scanning tunneling microscope (STM) tip and a gold surface, as reported in the August 29 issue of *Science*.

The molecular junctions were created in a liquid cell by repeatedly moving a gold

STM tip into and out of contact with the sample. In the first step, the formation of a chain of Au atoms was observed in pure solvents (toluene and water). The conductance of this chain decreased with increas-

Review Articles and Special Issues

Annals of Biomedical Engineering **31** (9) (October 2003) contains "Bioreactors for Cardiovascular Cell and Tissue Growth: A Review" by V. Barron, E. Lyons, C. Stenson-Cox, P.E. McHugh, and A. Pandit (p. 1017).

Applied Mechanics Reviews **56** (5) (September 2003) contains "Use of Conventional Optical Fibers and Fiber Bragg Gratings for Damage Detection in Advanced Composite Structures: A Review" by K.S.C. Kuang and W.J. Cantwell (p. 493) and "Recent Developments and Applications of Invariant Integrals" by Y.-H. Chen and T. J. Lu (p. 515).

Crystallography Reports **48** (5) (September 2003) contains "Magnetoplastic Effect: Basic Properties and Physical Mechanisms" by V.I. Alshits, E.V. Darinskaya, M.V. Koldaeva, and E.A. Petrzhih (p. 768); and "The Influence of Magnetic Effects on the Mechanical Properties and Real Structure of Nonmagnetic Crystals" by A.A. Urusovskaya, V.I. Alshits, A.E. Smirnov, and N.N. Bekkauer (p. 796).

Journal of Applied Physics **94** (8) (October 15, 2003) contains "Fluorescence Intensity Ratio Technique for Optical Fiber Point Temperature Sensing" by S.A. Wade, S.F. Collins, and G.W. Baxter (p. 4743).

Journal of Energy Resources Technology **125** (3) (September 2003) contains "Innovative Technologies for Managing Oil Field Waste" by J.A. Veil (p. 238).

Journal of Experimental and Theoretical Physics **97** (2) (August 2003) contains "Superconductivity in Doped Nondegenerate Insulators" by A.I. Agafonov and E.A. Manykin (p. 358) and "X-Ray Optical Activity: Applications of Sum Rules" by J. Goulon, A. Rogalev, F. Wilhelm, C. Goulon-Ginet, P. Carra, I. Marri, and Ch. Brouder (p. 402).

Journal of Microelectromechanical Systems **12** (4) (August 2003) contains "Surface Tension-Powered Self-Assembly of Microstructures—The State of the Art" by R.R.A. Syms, E.M. Yeatman, V.M. Bright, and G.M. Whitesides (p. 387).

Journal of Vacuum Science & Technology B: Microelectronics and Nanometer Structures **21** (5) (September 2003) contains "Review of Trench and Via Plasma Etch Issues for Copper Dual Damascene in Undoped and Fluorine-Doped Silicate Glass Oxide" by D.L. Keil, B.A. Helmer, and S. Lassig (p. 1969).

Physics of the Solid State **45** (10) (October 2003) contains "Band Structure and Properties of Superconducting MgB₂ and Related Compounds (A Review)" by A.L. Ivanovskii (p. 1829).

Review of Scientific Instruments **74** (10) (October 2003) contains "Recent Advancements in Microwave Imaging Plasma Diagnostics" by H. Park, C.C. Chang, B.H. Deng, C.W. Domier, A.J.H. Donné, K. Kawahata, C. Liang, X.P. Liang, H.J. Lu, N.C. Luhmann Jr., A. Mase, H. Matsuura, E. Mazzucato, A. Miura, K. Mizuno, T. Munsat, Y. Nagayama, M.J. van de Pol, J. Wang, Z.G. Xia, and W-K. Zhang (p. 4239).

Reviews of Modern Physics **75** (4) (October 2003) contains "Colloquium: Saturation of Electrical Resistivity" by O. Gunnarsson, M. Calandra, and J.E. Han (p. 1085); "Hamiltonian Theories of the Fractional Quantum Hall Effect" by G. Murthy and R. Shankar (p. 1101); and "How to Detect Fluctuating Stripes in the High-Temperature Superconductors"

by S.A. Kivelson, I.P. Bindloss, E. Fradkin, V. Oganessian, J.M. Tranquada, A. Kapitulnik, and C. Howald (p. 1201).

Semiconductors **37** (10) (October 2003) contains "Modification of Hg_{1-x}Cd_xTe Properties by Low-Energy Ions" by K.D. Mynbaev and V.I. Ivanov-Omskii (p. 1127).

IEEE Transactions on Semiconductor Manufacturing **16** (3) (August 2003) features a "Guest Editorial: Special Section on Compound Semiconductor Microelectronics Manufacturing: The Future is Here."

International Journal of Mass Spectrometry **229** (1–2) (September 2003) features "Mass Spectrometry Contributions to Nanosciences and Nanotechnology."

Journal of Biomedical Optics **8** (3) (July 2003) features a "Special Section on Multiphoton Microscopy."

Journal of Engineering Materials and Technology **125** (4) (October 2003) features a "Special Issue on Durability and Damage Tolerance of Heterogeneous Materials and Structures."

Journal of Microlithography, Microfabrication, and Microsystems **2** (4) (October 2003) features a "Special Section on Surface Micromachining" and a "Special Section on Micro-Optics for Photonic Networks."

Journal of Pressure Vessel Technology **125** (3) (August 2003) features a "Special Issue on Pressure Vessels Technology Applied to Gun Tubes."

Journal of Vibration and Acoustics **125** (4) (October 2003) features "Special Issue: The Contributions of Jørgen W. Lund to Rotor Dynamics."

Optical Engineering **42** (10) (October 2003) features a "Special Section on Advances in Optical Waveguide Engineering."

Applied Surface Science **219** (1–2) (October 15, 2003) contains "Proceedings of Applied Surface Modeling: Experiment, Theory and Simulations."

Cryogenics **43** (10–11) (October–November 2003) contains Proceedings of the Korea-Japan Joint Workshop 2002 on Applied Superconductivity and Cryogenics.

Infrared Physics & Technology **44** (5–6) (October–December 2003) contains Proceedings of the Workshop on Quantum Well Infrared Photodetectors.

Journal of Physics and Chemistry of Solids **64** (9–10) (September 2003) contains selected papers from the International Conference on Ternary and Multinary Compounds (ICTMC13).

Microelectronics Reliability **43** (9–11) (September–November 2003) contains Proceedings of the 14th European Symposium on Reliability of Electron Devices, Failure Physics, and Analysis.

Optical Materials **24** (1–2) (October–November 2003) contains Proceedings of the Fifth French-Israeli Workshop on Optical Properties of Inorganic Materials.

Solid-State Electronics **47** (10) (October 2003) contains papers selected from the 12th Workshop on Dielectrics in Microelectronics.

Thin Solid Films **442** (1–2) (October 1, 2003) contains selected papers from the 4th International Conference on Coatings on Glass.

ing tip distance in a stepwise fashion, with a step value equal to the quantum of conductance, until the conductance value almost reached zero. Additional steps with step values of approximately integral multiples of 1/100 of the conductance quantum were observed for 1 mM 4,4'-bipyridine in a 0.1 M NaClO₄ water solution. The researchers attribute these additional conductance steps to the formation of junctions with one, two, three, and more molecules. In order to confirm that the conductance steps were caused by the formation of stable molecular junctions, a solution of 2,2'-bipyridine molecules was tested. In 2,2'-bipyridine, the positions of

two nitrogen atoms prevent the molecule from simultaneously binding to two electrodes, and no conduction steps were observed. The same experiments were performed for hexanedithiol, octanedithiol, and decanedithiol molecules in toluene. The conductance showed stepwise behavior, but the step size was smaller than in the case of 4,4'-bipyridine because of the higher resistance of *N*-alkanedithiol molecules as compared with 4,4'-bipyridine. The researchers said that the resistance of *N*-alkanedithiol molecules corresponds well with the widely accepted model of electron tunneling through the molecule.

MAXIM NIKIFOROV

"Design Rules" of Silk Production Unraveled in Studies of *Bombyx mori* Cocoons

Traditionally, silk fibers produced by silkworms and spiders are harvested, disentangled, and then woven into fabrics. H.-J. Jin and D.L. Kaplan from Tufts University have begun to unravel the *in vitro* mechanism of silk processing in insects and spiders. As described in the August 28 issue of *Nature*, the researchers monitored the behavior of the silk fibroin solutions as a function of decreasing water content. Starting with the cocoons of the domestic silk moth *Bombyx mori*, the researchers "degummed" the cocoons to generate sericin-free fibroin fibers. The family of sericin proteins is hydrophilic and acts as the glue between fibroin fibers. The sericin in these aqueous fibroin solutions was substituted with polyethylene oxide (PEO). The silk fibroin and the PEO molecules preferentially vie for the water molecules in which the protein is dissolved. As the fibroin concentration is increased and the water content is lowered, micelles form first, ranging in diameter from 100 nm to 200 nm; subsequently, "globules" form as the water content is further decreased. Through scanning electron microscopy and atomic force microscopy, the researchers observed that these globules arise from phase separation between the hydrophilic and hydrophobic segments. Films of the fibroin aqueous solutions were cast and subsequently treated with methanol, physical shear, and stretching. The characteristics of the resulting silk structures depended critically upon the nature of the postprocessing.

The researchers describe a process that combines the primary sequence of the silk proteins and the biological environment of the gland during silk spinning to create silk fibers. These "design rules," said the researchers, apply to all silk proteins in terms of processing in aqueous environments, which can lead to materials engineering in aqueous systems of new silk-based materials with desired properties for potential applications in tissue engineering and biomaterials.

LARKEN E. EULISS

Carbon Nanocoil Supports Surpass Performance of Other Nanostructured Materials in Direct Methanol Fuel Cells

T. Hyeon of Seoul National University, Y.-E. Sung of Kwangju Institute of Science and Technology, and colleagues have developed carbon nanocoils as a catalyst support for the fabrication of direct methanol fuel-cell (DMFC) elec-

Cost-Effective Portable Spin Coater



Two-Stage Spinning

Dispense liquid during Stage 1
Spin-up and flatten during Stage 2

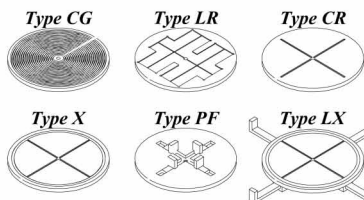
Adjustable Speed

Stage 1

500 to 2500 rpm
2 to 18 seconds

Stage 2

1,000 to 8,000 rpm
3 to 60 seconds



Vacuum Chucks

Wide Range of Vacuum Chucks Available To Hold Different Substrates in KW-4A Spin Coater

KW-4A SERIES PRODUCT LINE



UV Curer
KW-4AC

Hot Plate
KW-4AH

Spin Coater
KW-4A

Dispenser
KW-4AD



CHEMAT TECHNOLOGY, INC.
9036 Winnetka Avenue, Northridge, CA 91324
1-800-475-3628, Fax: 818-727-9477
website: www.enlabproducts.com; www.chemat.com
email: marketing@chemat.com

For more information, see <http://advertisers.mrs.org>

trodes. They synthesized the carbon nanocoils by heat-treating solid composites of a carbon precursor (resorcinol formaldehyde gel), silica sol, and a transition-metal salt. The research team said that because the synthetic procedure is simple and inexpensive, it can be readily applied to cost-effective, large-scale production of the material. High surface area and good crystallinity are the characteristics needed for the catalyst support for DMFCs. As the researchers reported in the September 22 issue of *Angewandte Chemie*, their synthesized carbon material exhibited a high surface area of 318 m²/g and was composed of 5–10-nm-thick graphitic coils. The crystallinity of the material was comparable to that of carbon nanotubes. The researchers said that this was especially important because it is difficult to obtain crystalline carbon materials with a large surface area. For example, they said, many activated carbons have surface areas exceeding 1000 m²/g, but they are noncrystalline and amorphous. Alternatively, graphite is highly crystalline, but has a very small surface area of <10 m²/g.

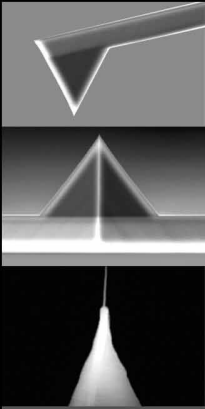
Carbon is a critical material for DMFCs because a good support exhibiting a homogeneous high dispersion of catalytic species is a key factor dominating the overall performance and stability of fuel cells. Hyeon and colleagues identified highly dispersed PtRu alloy catalysts of up to 60 wt% on their carbon support, resulting in higher catalytic activity for methanol oxidation. In a half-cell test for methanol oxidation at 0.6 V, the electrode using the carbon nanocoil had six times higher current than that of a commercialized fuel-cell carbon substrate.

The carbon nanocoil performed better as a support material for fuel cells than other nanostructured carbon materials. In particular, the nanocoils exhibited a current density that was three times higher at a given voltage than that of the graphitic carbon nanofiber, which was known to be one of the best catalyst supports for DMFC electrodes. In nanocoil experiments using a full fuel cell—composed of a cathode, anode, and polymer membrane electrolyte—the maximum power density increased by >85% over the standard commercial sample at 30°C.

Oxide Superlattices Containing Si Nanocrystals and Er Ions Luminesce Efficiently at 1.54 μm

M. Zacharias and colleagues from the Max Planck Institute of Microstructure Physics (Halle, Germany) have developed a means of controlling the size of silicon nanocrystals and custom-manufacturing these crystals on 4 in. wafers. The technique is based on a combination of superlattices—multilayer structures with layer thicknesses of a few nanometers and varying bandgaps—and phase separation in the ultrathin layers.

The superlattice structure of amorphous silicon oxide layers (SiO_x/SiO₂) was manufactured using a standard deposition technique. The researchers employed a variation of this technique by evaporating the silicon oxide either in a vacuum or in an oxygen-containing atmosphere. The resulting amorphous SiO/SiO₂ superlattice structure was then tempered in a nitrogen-containing atmosphere at 1100°C. Through the thermally activated phase separation, the SiO in the ultrathin sublayers transformed into pure silicon nanocrystals and amorphous SiO₂.



AFM PROBES

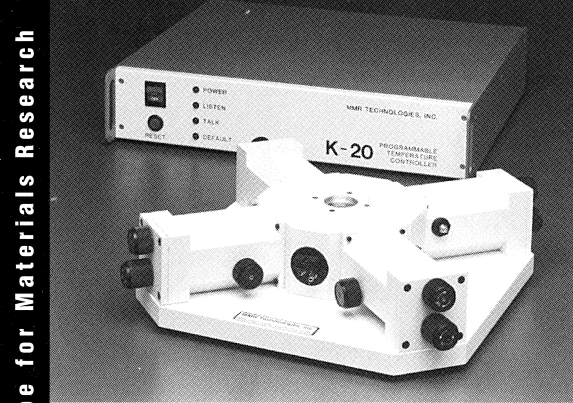
- ▶ Industry Standard
- ▶ High Quality
- ▶ Fast Delivery



ProbeStore.com

PACIFIC NANOTECHNOLOGY, INC.
3350 Scott Blvd #29, Santa Clara, CA 95054-3105
1-800-246-3704
Email: info@pacificnanotech.com
www.pacificnanotech.com

For more information, see <http://advertisers.mrs.org>



Variable Temperature Micro Probe for Materials Research

MMR's **Variable Temperature Micro Probe System** (one to seven probes) is designed to provide controlled cycling of sample temperature from 80K to 730K (450°C).

Applications Include:

- DLTS
- Four Point Resistivity Measurements
- MEMS
- Material Characterization Studies
- Electronic Device Characterization

For information, contact Bob Paugh at (650) 962-9620 or bobp@mmr.com.
Or visit our web page at <http://www.mmr.com>.

MMR **MMR Technologies, Inc.**

VISIT MRS BOOTH 1003

For more information, see <http://advertisers.mrs.org>

Metals & Materials from

www.goodfellow.com

**Faster
Better
Cheaper**

VISIT MRS BOOTH NO. 212

Find what you
need quickly

48,000 items
plus detailed
technical data

5% discount on
online orders

Goodfellow

Metals • Alloys • Ceramics • Polymers

1-800-821-2870

fax 1-800-283-2020

info@goodfellow.com

© 2003 Goodfellow Corporation

For more information, see <http://advertisers.mrs.org>

whereby the nanocrystals were automatically surrounded with an appropriate barrier material.

The size of the crystals within the range, for example, of 2–5 nm can be determined by the thickness of the layer. The distance between the crystals can be adjusted by varying the thickness of the SiO₂ barrier layers and the oxygen content of the SiO_x layers. A higher oxygen content would automatically lead to a higher proportion of the amorphous SiO₂ after the phase separation and thereby to a larger distance between the silicon nanocrystals within the sublayer. The luminescence of the silicon increases with the number of crystals, and the quantum efficiency of smaller crystals is higher than that of larger crystals; therefore, primarily very small crystals at high density

are required for the highest possible luminescence intensity.

The researchers said that when the nanocrystal structures are implanted with erbium ions, an effective energy transfer occurs from the nanocrystals to the Er³⁺ ions, and the luminescence shifts to ~1.54 μm. This particular wavelength is of technological importance, since the fiber-optic cable employed in optical data transmission exhibits a transmission maximum at 1.54 μm. Additionally, erbium-doped glass fiber is used as an amplifier for optical data transmission. Memory circuitry is another area of application of silicon nanocrystals in oxide matrices. The researchers submitted a patent for their technique for tailor-made silicon nanocrystals on 4 in. wafers.

A Spin-Transfer Switch for Magnetic Memory Spintronics?

Recent studies have demonstrated that when a spin-polarized electric current is passed through a ferromagnet a few nanometers thick, the nanomagnet experiences a large torque due to direct transfer of spin angular momentum. This allows the magnetic moment of the nanomagnet to oscillate at microwave frequencies around its symmetry axis until it reverses its orientation, thereby accomplishing a magnetic switch. D.C. Ralph of Yale University, S.I. Kiselev of Cornell University, and their co-researchers have demonstrated the nature of the physics behind this phenomenon. They reported their work in the September 25 issue of *Nature*.

The research team formed a 130 nm × 70 nm magnetic multilayered nanopillar with layers of magnetic Co and nonmagnetic Cu and Pt deposited on a silicon substrate. The multilayered composition was 80 nm Cu/40 nm Co/10 nm Cu/3 nm Co/2 nm Cu/30 nm Pt. A dc current bias was applied through a top Cu contact, and a static magnetic field was applied in the sample plane. The 40-nm-thick Co layer is referred to as the “fixed” layer because it is relatively insensitive to the applied magnetic field, whereas the 3 nm Co layer is referred to as the “free” layer because it is sensitive to the applied field. The electrons in the dc current were spin-polarized as they passed through the fixed layer. This spin-polarized current was then passed through the free layer. This subjected the magnetic moment of this layer to the spin-transfer torque, resulting in the emission of microwaves. When the researchers measured the microwaves and mapped the strength of the oscillations as a function of electric current and magnetic field, they revealed several types of magnetic excitation. The researchers said the only input was the dc electric current and the applied static magnetic field, while the output contained microwave emissions in a frequency range predicted by theory and prior calculations, clearly demonstrating the spin-transfer mechanism.

This study shows that the magnetic multilayered structure acts as a nanoscale motor, although there is no mechanical motion. Energy from the dc current was converted into high-frequency magnetic rotations. This work has implications for spintronic devices, such as magnetic memory devices. The researchers suggest that nanomagnets driven by spin-polarized currents could be used as tunable nanoscale microwave sources or oscillators.

GOPAL R. RAO

FOR MORE RESEARCH NEWS ON MATERIALS SCIENCE . . .

. . . access the Materials Research Society Web site:

www.mrs.org/gateway/matl_news.html